Structure-based design, synthesis, and biological activity evaluation of chalcone-piperazine derivatives as dual AChE and MAO B inhibitors

Berkant Kurban, [ID] [abc] Begüm Nurpelin Sağlık Özkan, [ID] [bd] Derya Osmaniye, [ID] [bd] Serkan Levent, [ID] [de] Yusuf Özkay [ID] [bd] and Zafer Asım Kaplancıklı [ID] *[bf]

The development of pharmaceutical compounds for the treatment of Alzheimer's Disease (AD) and other neurodegenerative diseases is crucial, as the pathophysiology of AD remains incompletely understood and effective treatments are still lacking. In this study, a series of novel compounds based on Donepezil, incorporating piperazine and chalcone structures, were designed, synthesized, and characterized. The structures of the compounds were confirmed using IR, ^{1}H-NMR, ^{13}C-NMR, and HRMS techniques. Biological activities of the compounds were evaluated against cholinesterase enzymes and monoamine oxidase enzymes. The most potent derivative against acetylcholinesterase (AChE) was compound **4g**, with an IC$_{50}$ value of 0.027 ± 0.001 μM, and the most potent against monoamine oxidase B (MAO B) was also **4g**, with an IC$_{50}$ value of 0.114 ± 0.003 μM. *In silico* studies further elucidated the interaction of compound **4g** with AChE. Molecular docking revealed key interactions between **4g** and amino acids in the AChE active site. A 100 ns molecular dynamics simulation confirmed the stability of the **4g**-AChE complex.

Introduction

Alzheimer's disease (AD) is a neurodegenerative disorder that directly affects brain functions responsible for abilities such as memory, speech, and thinking. Alzheimer's disease (AD) became known for the first time in literature when Alois Alzheimer discovered the illness in a 51-year-old female patient in 1901 and described it in 1906.[1] In addition, among all causes of death, AD ranks after conditions such as cancer and cardiovascular diseases, and it is undoubtedly the neurodegenerative disease that causes the most deaths.[2] According to the World Health Organization, it is expected that by 2050, there will be 139 million individuals with dementia, primarily due to Alzheimer's disease.[3] In the United States, 10.7% of people over the age of 65 have dementia due to AD[4] and this fatal disease causes the deaths of more than 10 000 people over the age of 65 in Turkey every year.[2,5]

There are various approaches to the treatment of AD. Several therapeutic classes, including cholinesterase (ChE) inhibitors, monoamine oxidase (MAO) inhibitors, and non-steroidal anti-inflammatory drugs, are currently employed or hold promise for future Alzheimer's disease (AD) management, targeting key pathological features such as β-amyloid deposition and reactive oxygen species. In addition, combinations of MAO inhibitors with other therapeutics, are being explored as promising combination therapies for the management of AD. In this study, synthesized compounds exhibiting both anti-ChE activity and MAO inhibition are considered highly valuable for the future treatment of AD.[6–10]

Although the pathophysiology of the disease has not yet been fully elucidated, there are various accepted approaches such as cholinergic hypothesis, amyloid hypothesis, neurodegenerative tauopathies and oxidative stress hypothesis. The cholinergic hypothesis, which emerged from the studies conducted by Bartus and colleagues in 1982, underpins the development of FDA-approved drugs such as Donepezil, Rivastigmine, and Galantamine, actively used in the treatment of AD. This hypothesis is distinguished from others by its unique characteristics and is based on observations of a decline in the cholinergic system among individuals with AD. It is theorized that this reduction in cholinergic activity leads to decreased levels of acetylcholine (ACh), resulting in learning and memory impairments. Consequently, enhancing ACh levels has been proposed as a strategy to restore cholinergic function. To increase ACh concentrations, inhibitors of the

[a]Department of Pharmaceutical Chemistry, Faculty of Pharmacy, Afyonkarahisar Health Sciences University, 03030 Afyonkarahisar, Turkey

[b]Department of Pharmaceutical Chemistry, Faculty of Pharmacy, Anadolu University, 26470 Eskişehir, Turkey. E-mail: zakaplan@anadolu.edu.tr

[c]The Institute of Graduate Education, Anadolu University, 26470 Eskişehir, Turkey

[d]Central Research Laboratory (MERLAB), Faculty of Pharmacy, Anadolu University, 26470 Eskişehir, Turkey

[e]Department of Analytical Chemistry, Faculty of Pharmacy, Anadolu University, 26470 Eskişehir, Turkey

[f]Pharmacy Services, Vocational School of Health Services, Bilecik Şeyh Edebali University, 11000 Bilecik, Turkey

acetylcholinesterase (AChE) enzyme, which breaks down ACh, are employed.[11–13]

The primary recognized function of ChE enzymes is to hydrolyze ACh. These enzymes are categorized into AChE (EC 3.1.1.7) and butyrylcholinesterase (BChE, EC 3.1.1.8). AChE plays a crucial role in the pathophysiology of neurodegenerative diseases, such as Alzheimer's disease (AD), due to its role in metabolizing ACh. Reduced levels of AChE are observed in some neurodegenerative conditions and are associated with the accumulation of pathological proteins, oxidative stress, apoptosis, and other phenomena prevalent in neurological disorders.[14–18]

In the healthy human brain, the activity of AChE suppresses that of BuChE. The most important feature that distinguishes BuChE from AChE is its kinetic response to ACh concentrations. At low ACh concentrations, BChE is less effective in ACh hydrolysis. However, at high ACh concentrations, where AChE activity is inhibited, BuChE becomes more active in AD, a marked reduction of AChE levels has been observed in specific brain regions even during the early stages of the disease. Concurrently, particularly the G1 form of BuChE increases as the disease progresses. This shift causes BuChE to assume the primary role in the hydrolysis of ACh, a role that is auxiliary in healthy individuals. Therefore, inhibiting BuChE in AD is crucial for maintaining the balance of ACh levels.[19]

Donepezil reversibly inhibits the AChE in the treatment of AD. It is also known to inhibit BuChE enzymes, albeit to a lesser extent than its inhibition of AChE enzymes. Donepezil, taken orally, readily crosses the blood–brain barrier. Donepezil, which is used in the treatment of mild or moderate AD, has been reported to have positive effects in severe cases despite its gastrointestinal side effects. Due to its high efficacy and status as one of the few molecules approved by FDA for the treatment of AD, Donepezil is frequently used as a reference molecule in research on AChE inhibitors and was selected as the reference molecule for this study.[4,20,21]

MAO (EC 1.3.3.4) is an essential enzyme in the breakdown of xenobiotic amines and monoamine neurotransmitters.[22] Most mammalian tissues contain two MAO isoenzymes; MAO A and MAO B. MAO A is inhibited at low concentrations by clorgyline and catalyses the oxidation of norepinephrine and serotonin. Meanwhile, non-polar aromatic amines without hydroxyl groups, like phenylamine, benzylamine, etc. are commonly targeted by MAO B. MAO B largely deaminates dopamine, prefers to use 2-phenylethylamine and benzylamine as substrates and is irreversibly inhibited at low concentrations by L-deprenyl (selegiline).[23] Therapeutic targets for the treatment of neuropsychiatric and neurodegenerative illnesses include both isoforms.[22,24]

The reaction catalyzed by MAO produces hydrogen peroxide, which may contribute to the formation of reactive oxygen species (ROS). This indicates that MAO activity could potentially result in neurotoxic effects. Enzymes such as catalase and superoxide dismutase typically metabolize ROS and other reactive species; however, dysfunction in these enzymatic systems can contribute to neurological disorders. Consequently, MAO inhibitors may be beneficial in treating

conditions like stroke and other forms of oxidative stress-related tissue damage.[23,25,26] MAO B inhibitors, selegiline and rasagiline, are used to treat Parkinson's disease and some novel selective MAO B inhibitors are critical for the treatment of neurodegenerative illnesses, particularly AD due to their effectiveness and few side effects. On the other hand MAO A inhibitors are primarily used as antidepressants and anxiolytics.[9,27,28]

Numerous studies have focused on compounds with multiple effects, as opposed to those that solely inhibit the AChE, BChE, or MAO B enzymes. Research has demonstrated that inhibiting more than one enzyme with a single molecule offers numerous advantages.[29–31]

Piperazine is a member of 6-membered diazocyclo alkane class with two secondary nitrogen atoms. Piperazine can interact with target enzymes through hydrogen bonds due to its non-planar flexible structure. Many pharmaceutically active substances across various indication groups incorporate piperazine in their structure. Due to its hydrophobic nature, piperazine is frequently utilized in research on treatments for AD, Parkinson's disease, and other neurodegenerative diseases, as it aids in crossing the blood–brain barrier.[32,33]

Chalcone structures are α, β-unsaturated ketones that contain a three-carbon α,β-unsaturated carbonyl system that connects two aromatic rings. The chalcone structure, serving as a binder within the molecule, not only prevents neuro-inflammation, amyloid, and tau accumulation but also underpins the development of compounds with diverse activities. It is known that compounds containing chalcone structures selectively inhibit MAO B activity.[32–35]
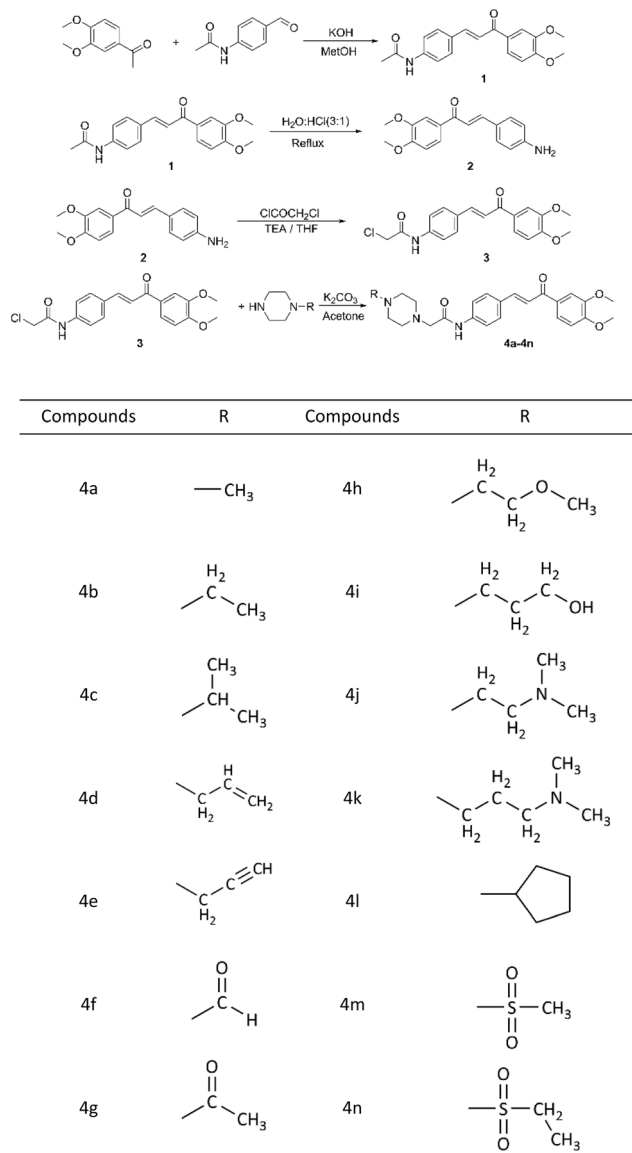
In this study, the structure–activity relationships of pharmacophore groups with previously demonstrated activity in the molecular design process were investigated. By combining these groups with necessary modifications, 14 new compounds featuring piperazine and chalcone structures were designed and synthesized. Their structures were elucidated, and their biological activities were evaluated. Current literature data were utilized during the design and synthesis processes. The synthesis of the compounds was carried out in four steps. IR, ¹H-NMR, ¹³C-NMR, and HRMS techniques were employed for structural elucidation. The effects of the obtained compounds on the enzymes AChE, BChE, MAO A, and MAO B were examined. To support these findings, molecular docking, and molecular dynamics studies were performed.

Results and discussion

Chemistry

Compounds **4a–4n** were obtained by following the procedure outlined in Scheme 1. In the first step, 3,4-dimethoxyacetophenone reacted with 4-acetamidobenzaldehyde to produce 3-(4-aminophenyl)-1-(3,4-dimethoxyphenyl)prop-2-en-1-one (**1**). In the next step, compound (**1**) underwent acidic hydrolysis with hydrochloric acid, yielding 3-(4-aminophenyl)-1-(3,4-dimethoxyphenyl)prop-2-en-1-one (**2**). Finally, acetylation of compound (**2**) with chloroacetyl chloride resulted in the formation of 2-chloro-N-(4-(3-(3,4-dimethoxyphenyl)-3-oxoprop-1-en-1-yl)acetamide (**3**). Target compounds were synthesized

Scheme 1 Synthesis pathway for obtained compounds (**4a–4n**).

in the fourth and final stage, which involved the reaction of 2-chloro-N-(4-(3-(3,4-dimethoxyphenyl)-3-oxoprop-1-en-1-yl) acetamide) (**3**) with piperazine derivatives. The structures of the obtained compounds were determined using spectroscopic techniques such as HPLC, FTIR, ^{1}H-NMR, ^{13}C-NMR, and HRMS. The data provided in the SI data.

Upon examination of the ^{1}H-NMR data, the expected number of peaks and chemical shift values were observed, consistent with the number of protons in the synthesized compounds. The peaks corresponding to the protons belonging to the piperazine ring and amide group in the obtained structures were observed in the expected regions. The protons belonging to the piperazine ring were observed as multiplet or broad peaks between 2.26 ppm and 3.72 ppm. The ^{1}H-NMR data of the piperazine ring were compared with literature values and found to be consistent.[36]

Upon analysis of the ^{13}C-NMR data of the obtained compounds, the characteristic peaks of amide carbonyls (C=

O), chalcone carbonyls (C=O) and methoxy groups (C–O) were prominently observed respectively; 168.90 ppm and 169.13 ppm, 187.64 ppm and 187.66 ppm, and 56.04 ppm and 56.26 ppm. In addition to these specific peaks, the peaks for aromatic carbons were observed at 111.07 ppm and above, while the peaks for aliphatic carbons appeared at 79.94 ppm and below. Apart from all these, in the most active compound **4g**, a distinct peak at 168.99 ppm was observed, corresponding to the acetyl carbonyl group, in addition to the other carbonyl groups.

Anticholinesterase enzyme activity studies

Donepezil, the reference molecule, had an AChE inhibition of $99.156 \pm 1.302\%$ at a concentration of 1×10^{-3} M. At 1×10^{-3} M, the inhibition of AChE was $93.462 \pm 3.162\%$ for compound **4a**, $92.641 \pm 2.447\%$ for compound **4b**, $96.805 \pm 2.926\%$ for compound **4f**, $98.027 \pm 2.557\%$ for compound **4g**, $90.641 \pm 2.745\%$ for compound **4h**, $94.168 \pm 2.062\%$ for compound **4i**, $94.027 \pm 1.938\%$ for compound **4j**, $97.449 \pm 2.811\%$ for compound **4k**, $89.361 \pm 2.590\%$ for compound **4m**, and $88.928 \pm 3.148\%$ for compound **4n**. As seen above, more than half of all synthesized compounds exceeded 90% inhibition. Donepezil, had an inhibition of $97.395 \pm 1.255\%$ at a concentration of 0.1×10^{-4} M. At 0.1×10^{-4} M, the inhibition of AChE was $90.251 \pm 1.862\%$ for compound **4a**, $88.667 \pm 2.235\%$ for compound **4b**, $94.837 \pm 3.957\%$ for compound **4f**, $96.441 \pm 2.499\%$ for compound **4g**, $90.469 \pm 2.827\%$ for compound **4i**, $92.154 \pm 3.484\%$ for compound **4j**, $94.087 \pm 2.963\%$ for compound **4k**, $87.648 \pm 1.718\%$ for compound **4m**, and $85.791 \pm 1.397\%$ for compound **4n**. These compounds advanced to the second stage for calculating IC$_{50}$ values for the AChE enzyme. Upon examining the results, most of the compounds showed IC$_{50}$ values below 0.1 μM. The IC$_{50}$ concentration of compound **4a** was determined as 0.068 ± 0.003 μM, the IC$_{50}$ concentration of compound **4f** as 0.048 ± 0.002 μM, the IC$_{50}$ concentration of compound **4g** as 0.027 ± 0.001 μM, the IC$_{50}$ concentration of compound **4j** as 0.043 ± 0.002 μM and the IC$_{50}$ concentration of compound **4k** as 0.039 ± 0.001 μM. In addition, the obtained compounds inhibited the BChE enzyme between $30.184 \pm 1.126\%$ and $45.967 \pm 1.921\%$ at a concentration of 1×10^{-3} M. At 0.1×10^{-4} M concentration, this range was $20.119 \pm 0.964\%$ to $33.314 \pm 1.221\%$ (Table 1).

Monoamine oxidase enzyme activity studies

Selegiline, selected as the reference compound for MAO B inhibition, had an inhibition rate of $98.589 \pm 2.055\%$ at a concentration of 1×10^{-3} M. At 1×10^{-3} M, the inhibition of MAO B was $83.952 \pm 1.925\%$ for compound **4a**, $60.441 \pm 2.269\%$ for compound **4b**, $78.228 \pm 2.484\%$ for compound **4e**, $90.749 \pm 2.620\%$ for compound **4f**, $92.322 \pm 2.160\%$ for compound **4g**, $79.462 \pm 2.864\%$ for compound **4h**, $74.137 \pm 2.422\%$ for compound **4i**, $82.248 \pm 3.026\%$ for compound **4j**, $58.035 \pm 1.628\%$ for compound **4m**, and $52.948 \pm 1.774\%$ for compound **4n**. Selegiline, had an inhibition rate of $94.850 \pm 1.114\%$ at a concentration of 0.1×10^{-4} M. At 0.1×10^{-4} M, the inhibition of MAO B was $80.528 \pm 2.240\%$ for compound **4a**, $88.62 \pm$

Table 1 % inhibition rates of the obtained compounds against AChE and BChE enzymes at 10^{-3} and 10^{-4} M concentrations and IC_{50} values

| Compound | AChE % inhibition | | | BChE % inhibition | | | |
	10^{-3} M	IC_{50} (M)	AChE	IC_{50} (M)	10^{-4} M	BChE	Selectivity and indexes
4a	93.462 ± 3.162	90.251 ± 1.862	0.068 ± 0.003	42.462 ± 1.852	24.558 ± 0.974	>1000	AChE/>1000
4b	92.641 ± 2.447	88.667 ± 2.235	0.093 ± 0.003	31.141 ± 1.034	27.034 ± 0.877	>1000	AChE/>1000
4c	79.168 ± 3.028	48.248 ± 1.984	>100	45.967 ± 1.921	25.474 ± 1.098	>1000	AChE/>10
4d	80.719 ± 3.339	40.020 ± 1.019	>100	40.328 ± 1.205	20.119 ± 0.964	>1000	AChE/>10
4e	67.223 ± 2.110	39.369 ± 1.320	>100	38.019 ± 0.964	21.922 ± 0.835	>1000	AChE/>10
4f	96.805 ± 2.926	94.837 ± 3.957	0.048 ± 0.002	31.703 ± 1.366	24.336 ± 0.829	>1000	AChE/>1000
4g	98.027 ± 2.557	96.441 ± 2.499	0.027 ± 0.001	36.426 ± 0.954	29.884 ± 0.920	>1000	AChE/>1000
4h	90.641 ± 2.745	86.522 ± 1.351	0.120 ± 0.005	30.184 ± 1.126	21.467 ± 0.874	>1000	AChE/>1000
4i	94.168 ± 2.062	90.469 ± 2.827	0.084 ± 0.003	39.637 ± 1.336	23.619 ± 1.069	>1000	AChE/>1000
4j	94.027 ± 1.938	92.154 ± 3.484	0.043 ± 0.002	42.719 ± 2.055	28.438 ± 1.156	>1000	AChE/>1000
4k	97.449 ± 2.811	94.087 ± 2.963	0.039 ± 0.001	45.952 ± 1.874	29.020 ± 1.039	>1000	AChE/>1000
4l	76.855 ± 2.357	40.323 ± 1.820	>100	41.008 ± 1.998	32.733 ± 1.354	>1000	AChE/>10
4m	89.361 ± 2.590	87.648 ± 1.718	0.158 ± 0.006	37.346 ± 0.961	33.314 ± 1.221	>1000	AChE/>1000
4n	88.928 ± 3.148	85.791 ± 1.397	0.205 ± 0.009	30.416 ± 0.823	24.764 ± 0.954	>1000	AChE/>1000
Donepezil	99.156 ± 1.302	97.395 ± 1.255	0.0201 ± 0.0014	—	—	—	
Tacrine	—	—	—	99.827 ± 1.378	98.651 ± 1.402	0.0064 ± 0.0002	

1.829% for compound **4f**, and 89.154 ± 2.168% for compound **4g**. The IC_{50} values of compounds **4a**, **4f** and **4g** obtained less than 1 μM and are similar to the reference molecule, selegiline. The IC_{50} concentration of compound **4a** was determined as 0.274 ± 0.012 μM, the IC_{50} concentration of compound **4f** as 0.137 ± 0.005 μM, and the IC_{50} concentration of compound **4g** as 0.114 ± 0.003 μM. Among the synthesized compounds, those containing groups with relatively smaller spatial volumes, such as methyl, aldehyde, or acetyl groups, were the most active. However, when the compounds contain long-chain groups such as isopropyl, dimethylaminopropyl, methylsulfonyl, or ethylsulfonyl, which occupy a relatively larger spatial volume, a significant decrease in their activity is observed. Compound **4g**, with an IC_{50} value of 0.114 ± 0.003 μM against the MAO B enzyme, was the most active compound against MAO B, similar to its activity against ChE enzymes. The high inhibitory activity

of compound **4g** against both AChE and MAO B enzymes demonstrates its multiple inhibitory properties (Table 2).

Kinetic studies of AChE enzyme inhibition

Enzyme kinetics studies were conducted to determine the mechanism of inhibition of AChE using a procedure similar to that of the inhibition assay for cholinesterase enzymes. These studies were performed with compound **4g**, which was found to be the most potent agent. Linear Lineweaver–Burk graphs were used to estimate the type of inhibition of this compound. The velocity curves of the substrates were recorded in the absence and presence of compound **4g**. This compound was prepared for enzyme kinetic studies at concentrations of $IC_{50}/2$, IC_{50}, and $2 \times IC_{50}$. In each case, the initial velocity measurements were obtained at different substrate (ATC) concentrations ranging from 600 to 18.75 μM. To calculate the K_i (intercept on the x-

Table 2 % Inhibition rates of the obtained compounds against MAO A and MAO B enzymes at 10^{-3} and 10^{-4} M concentrations and IC_{50} values

| Compound | MAO A % inhibition | | | MAO B % inhibition | | | |
	10^{-3} M	10^{-4} M	MAO A IC_{50} (M)	IC_{50} (M)	10^{-4} M	MAO B IC_{50} (M)	Selectivity and indexes
4a	47.664 ± 2.041	38.722 ± 1.061	>1000	83.952 ± 1.925	80.528 ± 2.240	0.274 ± 0.012	MAO-B/>1000
4b	53.118 ± 2.165	31.167 ± 1.236	>100	60.441 ± 2.269	40.103 ± 1.969	>100	—
4c	47.429 ± 0.836	39.049 ± 0.933	>1000	41.137 ± 0.941	28.864 ± 1.023	>1000	—
4d	55.003 ± 2.057	41.428 ± 1.958	>100	36.664 ± 1.037	30.097 ± 0.957	>1000	MAO-A/>10
4e	61.367 ± 1.949	44.213 ± 1.874	>100	78.228 ± 2.484	39.310 ± 1.484	>100	—
4f	40.841 ± 0.955	28.802 ± 0.861	>1000	90.749 ± 2.620	88.628 ± 1.829	0.137 ± 0.005	MAO-B/>1000
4g	68.957 ± 2.516	39.367 ± 1.108	>100	92.322 ± 2.160	89.154 ± 2.168	0.114 ± 0.003	MAO-B/>1000
4h	59.864 ± 2.241	28.558 ± 1.047	>100	79.462 ± 2.864	41.320 ± 0.916	>100	—
4i	41.110 ± 2.058	29.067 ± 0.962	>1000	74.137 ± 2.422	47.436 ± 1.623	>100	MAO-B/>10
4j	47.657 ± 1.936	32.294 ± 1.141	>1000	82.248 ± 3.026	40.124 ± 1.057	>100	MAO-B/>10
4k	63.049 ± 2.857	41.311 ± 1.936	>100	48.691 ± 1.839	36.087 ± 0.964	>1000	MAO-A/>10
4l	36.726 ± 0.984	30.430 ± 1.247	>1000	46.720 ± 1.154	29.702 ± 0.841	>1000	—
4m	39.430 ± 1.369	33.625 ± 1.320	>1000	58.035 ± 1.628	28.989 ± 0.826	>100	MAO-B/>10
4n	44.974 ± 1.955	24.118 ± 0.933	>1000	52.948 ± 1.774	27.841 ± 1.174	>100	MAO-B/>10
Moclobemide	94.121 ± 2.760	82.143 ± 2.691	6.0613 ± 0.2625	—	—	—	
Selegiline	—	—	—	98.589 ± 2.055	94.850 ± 1.114	0.0374 ± 0.0016	

axis) values of this compound value, the secondary plots of slope (K_m/V_{max}) *versus* varying concentrations (0, $IC_{50}/2$, IC_{50}, and $2 \times IC_{50}$) were created. The graphical analyses of steady-state inhibition data for compound **4g** are shown in Fig. 1.

According to the Lineweaver–Burk plots, the type of inhibition consists of two general classes: reversible or irreversible. Mixed-type, uncompetitive, competitive, and noncompetitive inhibition types are included in the reversible inhibition.[37–39] As seen in the Lineweaver–Burk plot of compound **4g** (Fig. 1), a graph with lines that do not intersect at the *x*-axis or the *y*-axis was formed. This observation indicated that compound **4g** was a reversible and mixed-type inhibitor with similar inhibition features as the substrates. Furthermore, the K_i value of compound **4g** was calculated as 0.047 μM with the help of a secondary plot.

Cytotoxicity assay

As a result of the cytotoxicity studies, the IC_{50} value of compound **4g** was found to be 32.18 μM (Table 3). Based on the relevant result, it is clear that compound **4g** is not cytotoxic.

Molecular docking

Among the compounds obtained in this study, compound **4g**, which demonstrated the highest activity, particularly in AChE enzyme inhibition, was subjected to docking studies with the

Fig. 1 (A) Lineweaver–Burk plots for the inhibition of AChE by compound **4g**. [S], substrate concentration (M); *V*, reaction velocity (1/V (abs per min)). Inhibitor concentrations are shown at the left. (B) Secondary plot for the calculation of the steady-state inhibition constant (K_i) of compound **4m**. K_i was calculated as 0.047 μM.

Table 3 IC_{50} value (μM) of compound **4g** against NIH/3T3 cell lines

Compound	NIH/3T3
4g	32.18
Doxorubicin	>1000

crystal structure of the AChE enzyme (PDB code: 4EY7) to elucidate its potential interactions with the enzyme's active site. While the crystal structure was preferred for these studies carried out in the light of current literature information, the *Homo sapiens* class was preferred due to the presence of Donepezil ligand and both packages of the enzyme active site.

During the studies, the "Glide 7.1" program was used for the docking technique, while the most probable poses were obtained with "GlideScore Sp". In addition, the electrostatic and Van der Waals interactions of the relevant compound of **4g** with the amino acids in the enzyme active site were displayed through the "Perresidue interaction" panel (Fig. 2).

Two different binding sites, the catalytic site (CAS) and the peripheral anionic site (PAS), must be considered when considering inhibitory activity for the AChE enzyme since the compounds that successfully settle into the passage formed by the CAS and PAS regions have high AChE enzyme inhibition values. It is known that for high inhibition values, interaction must be established with various amino acids located in both regions; Phe338, Tyr337, Tyr133, Tyr130, Trp86, His447, Glu334 and Ser203 for the CAS region, and Trp286, Tyr341, Tyr124, Asp74 and Tyr72 are of great importance in binding to the PAS region.[40–42]

Donepezil was our lead molecule in our molecular docking study because of its binding with both the PAS and CAS regions of the AChE enzyme, its use in AD treatment, and its activity values. Donepezil's dimethoxy indanone group had a π–π interaction with the Trp286 amino acid located in the PAS region of the AChE enzyme. Additionally, Donepezil forms a hydrogen bond with the Phe295 amino acid in the same region, and its dimethoxy indanone group and mono-substituted benzene ring also have a π–π interaction with the Trp86 amino acid in the CAS region of the AChE (Fig. 3).

Among the synthesized compounds, those with long chains, branches, and groups occupying relatively more space were less successful in molecular docking studies than those with shorter chains and groups occupying relatively less space. The main reason is that the compounds with long chains, branches, and bulky groups occupy too much space and, due to their structure, cannot form effective bonds with both regions of the AChE enzyme.

It is observed that compound **4g**, like Donepezil, forms bonds by settling into both the CAS and PAS regions of the enzyme. This interaction with both regions, a hallmark of AChE inhibitors especially notable in Donepezil, holds true for compound **4g** as well. Consequently, compound **4g** achieved successful results in biological activity tests. The dimethoxyphenyl group in compound **4g** engages in π–π interactions with the amino acid Trp286, similar to those observed in Donepezil. Such interactions are critical for activity on the AChE enzyme, making their observation
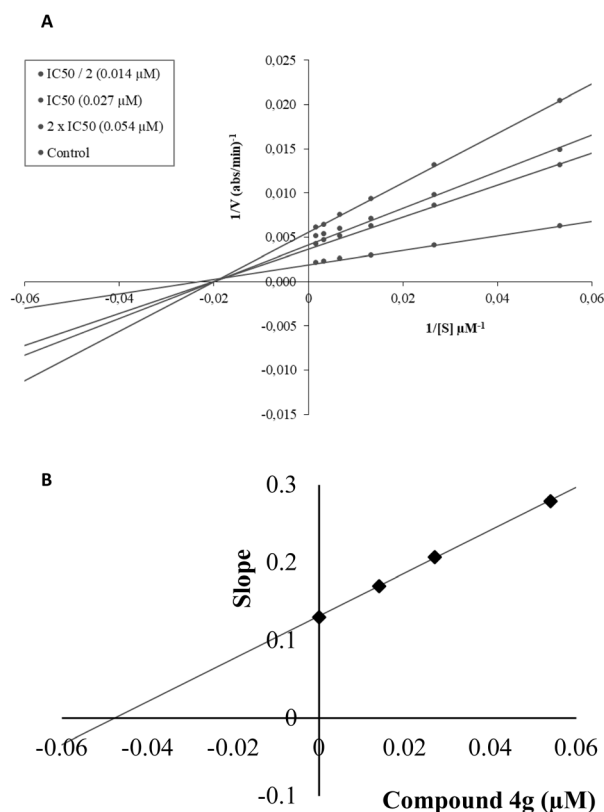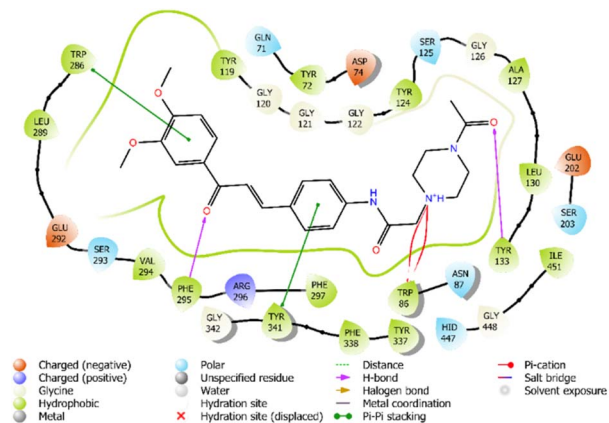
Fig. 2 Two-dimensional view of the interaction of compound **4g** with the active site of the AChE enzyme.
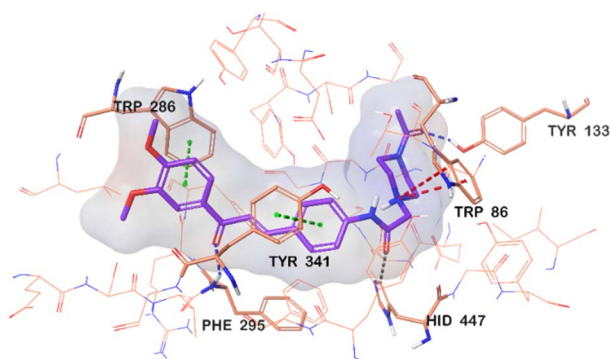

Fig. 3 Three-dimensional view of the interaction of compound **4g** with the active site of the AChE enzyme.

particularly significant given the design objectives of these compounds. The hydrogen bond between the chalcone group of the compound **4g** and the amino acid Phe295, a key factor in the binding to the enzyme's active site, was also observed. The observation of this interaction in molecular docking studies of compound **4g** is a very positive finding regarding the binding of the compound to the enzyme active site.

A π–π interaction was observed between the benzene ring of compound **4g** and the amino acid Tyr341, which plays a crucial role in binding to the enzyme's active site. The interaction of compound **4g** with the relevant amino acid is very important in terms of the activity of the compound on the AChE enzyme.

It was determined that compound **4g** formed a hydrogen bond with the amino acid Tyr133 in the CAS region of the enzyme. Distinguishing it from other compounds, the acetyl group within its structure interacts with Tyr133, explaining why compound **4g** excels in biological activity studies. Additionally, the nitrogen atom in the piperazine group, situated near the amide and chalcone groups, catalyzes a π–cation interaction with the Trp86 amino acid, also in the CAS region.

Molecular dynamics simulation

The molecular dynamics simulation approach is widely utilized to understand the dynamic behaviour of proteins or protein–

ligand complexes. In this study, a 100 ns MD simulation analysis was conducted in an open hydration environment to assess the stability of the complex formed between AChE (PDB ID: 4EY7) and the promising molecular compound **4g** and simulation results shown in Fig. 4 and 5. The stability of the model developed during the molecular dynamics simulation was evaluated using the RMSD (root mean square deviation of atomic positions) and RMSF (root mean square fluctuation) parameters. During the simulations, the stability of the created model was checked *via* the RMSD parameter. Fig. 4(A) shows the RMSD plot as a function of simulation time. The target range for RMSD values is between 1 and 3. Since the RMSD value in the obtained graph is within the relevant range (max 2.7 Å), it is possible to say the stability of the created model is preserved. The RMSD value increases and fluctuates until reaching 40.20 ns, where it stabilizes around this point. When the changes occurring during this fixation time were examined (Fig. 5B), it was seen that the interactions between compound **4g** and the amino acids Gly121, Ser125, Tyr133, Tyr337 and His447 started and strengthened. Therefore, it is thought that this amino acid contributes to stability. According to the AChE-**4g** complex protein RMSD analysis, the simulated system was stabilized quite effectively.

In molecular dynamics studies, the stability of the protein–ligand complex is significantly influenced by specific amino acids. During modelling, individual residue variation and structural changes along the protein chain can be observed using the RMSF parameter (Fig. 4B). In the RMSF graphic, α-
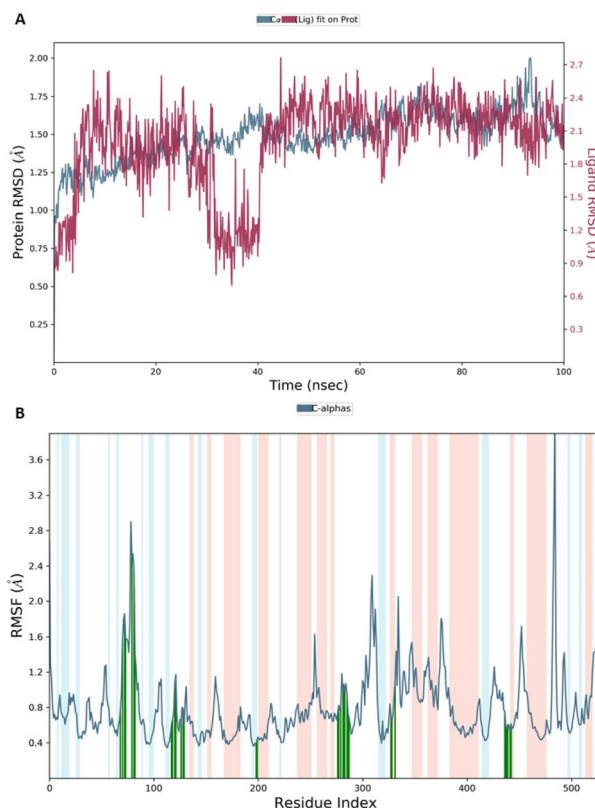

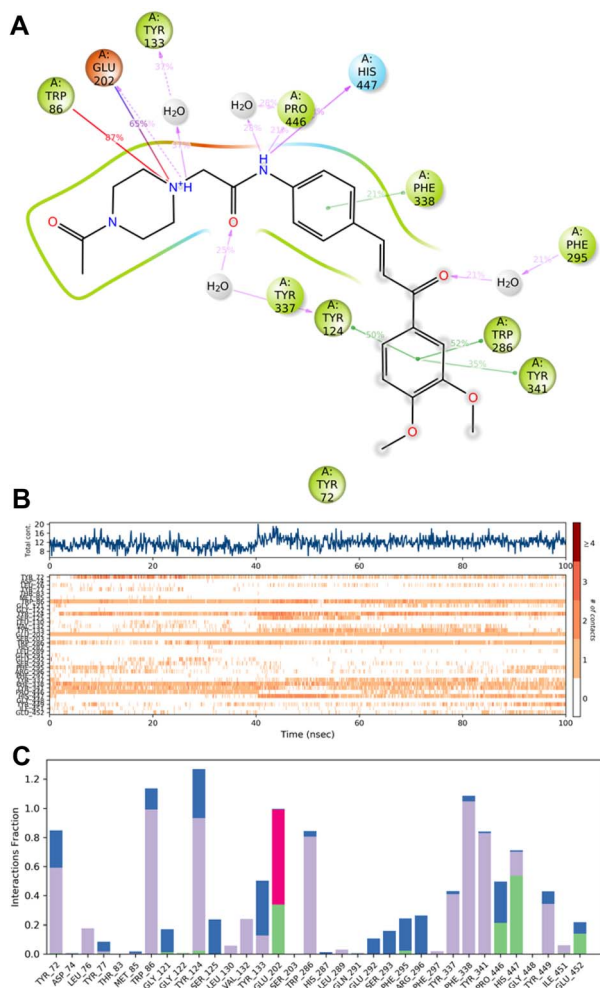**Fig. 4** MD simulation results performed with the compound **4g**-AChE complex (A and B).

Fig. 5 MD simulation results performed with the compound **4g**-AChE complex (A–C).

helix areas are shown by red, β-banded regions are represented by blue, and the loop region is represented by white. The α-helical and β-sheet portions of the protein are stiffer than the loop area resulting in fewer fluctuations in these regions. On the plot's X-axis, vertical green lines indicate the contributions of contacting residues between each protein chain and the ligand.

Compound **4g** interacts with 36 amino acids of the AChE protein, according to the RMSF study. These amino acids can be listed as follows: Tyr72, Asp74, Thr75, Leu76, Tyr77, Thr83, Met85, Trp86, Gly121, Gly122, Tyr124, Ser125, Leu130, Val132, Tyr133, Glu202, Ser203, Trp286, His287, Leu289, Gln291, Glu292, Ser293, Val294, Phe295, Arg296, Phe297, Tyr337, Phe338, Tyr341, Phe446, His447, Gly448, Tyr449, Ile451, Glu452. In the AChE-**4g** complex, there is no significant change in the resulting RMSF plot fluctuations.

Aromatic hydrogen bonds formed during a 100 ns molecular dynamics simulation were analyzed by reviewing the simulation video. It was observed that compound **4g** establishes aromatic hydrogen bonds with the amino acids Tyr72, Gly122, Tyr124, Phe297, Tyr337, and Tyr449. Specifically, the benzene rings in compound **4g** form aromatic hydrogen bonds with the carbonyl

groups of Gly122, Tyr124, Phe297, and Tyr337. Additionally, the methoxy groups on the dimethoxybenzene ring of compound **4g** engage in aromatic hydrogen bonding with the phenyl ring of Tyr72. Lastly, a similar interaction occurs between the carbonyl group adjacent to the piperazine ring in compound **4g** and the phenyl ring of Tyr449.

Interaction of compound **4g** with amino acids in the active site can be seen in Fig. 5(A–C). The amino acids that interact with the enzyme active site more than 20% are displayed in Fig. 5(A). The interaction number and residue graph are shown in Fig. 5(B). In this figure, compound **4g** is shown to interact consistently with Trp86, Tyr124, Glu202, Trp286 and Phe338. The interaction with amino acids Gly121, Ser125, Tyr133, Tyr337, and His447 began around 40.20 ns and continued mostly uninterrupted, playing a crucial role in ensuring stability. The consistent interaction with amino acids Trp86, Glu202, Trp286, Tyr337, Phe338, and His447, which are particularly critical for the AChE enzyme active site, further underscores the compound's potential. The interaction fractions with respect to the residue during the simulation are displayed in Fig. 5(C) (green: H-bond, pink: ionic interaction, purple: hydrophobic interaction, blue: water-mediated H-bond). In this figure, interactions with amino acids that are important for the enzyme active site are clearly seen.

Structure–activity relationships

The compounds **4a–4n** synthesized in this study are composed of three distinct regions; while the second and third regions have the same structure in 14 different compounds synthesized, and these compounds were derivatized over the substituents of the piperazine ring in the first region. Upon examining the main skeleton of the compounds, it can be observed that the first region features a piperazine ring and an acetamide structure. The related region of Donepezil interacts with the CAS region of the AChE enzyme and contributes significantly to the AChE inhibitory activity of Donepezil. Studies have demonstrated that for the inhibition of the AChE enzyme, the presence of heterocyclic structures like piperazine in the sections of compounds that interact with the CAS region of the AChE enzyme positively influences their activity. Secondary amines in the first region of the compounds are known to be effective hydrogen donors. Therefore, when the synthesized compounds encounter enzymes such as AChE, the secondary amines within the compounds engage in interactions that enhance their activity (Fig. 6).

The second region of the synthesized compounds consists of the benzene ring, labeled as ring A from the chalcone group, and a two-carbon unsaturated chain also belonging to the chalcone group. The second region acts as a link between the first and third regions. During the design process of the compounds, the chalcone structure was selected for the second region, which serves as a linking element, because it was intended to target multiple effects on both MAO B and cholinesterase enzymes. This choice was made because compounds containing chalcone groups in their structures are known to induce selective inhibition of MAO B.[43]
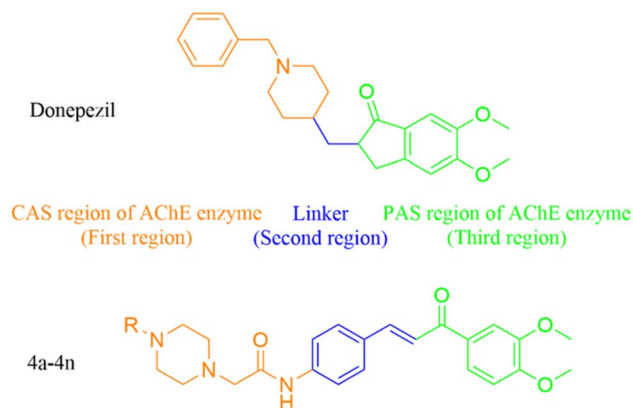
Fig. 6 Comparison of target compounds with donepezil.

In the third region of the synthesized compounds, the benzene ring, labeled as ring B, features methoxy groups substituted at the third and fourth positions, along with a carbonyl group belonging to the chalcone group. Compared to Donepezil, this region corresponds to where the indanone ring system is located in Donepezil. For AChE inhibitors and inhibitor candidate compounds, particularly Donepezil, the presence of two adjacent methoxy groups significantly enhances activity. Given that the indanone ring system of Donepezil interacts with the PAS of the AChE enzyme, the third region of the synthesized compounds is also expected to interact with the PAS site of the AChE enzyme.[44,45]

Among the compounds obtained, compounds **4c**, **4d**, **4e** and **4l** showed the lowest activity on the AChE enzyme. It is thought that a decrease in the AChE enzyme inhibition values of the relevant compounds occurs because the isopropyl, allyl, propine, and cyclopentyl groups substituted on the piperazine rings do not establish effective interactions with the CAS of the AChE enzyme. Due to their structural characteristics, these groups can not interact effectively with both the CAS and PAS active sites. The IC$_{50}$ values of **4a**, **4f**, **4g**, **4j** and **4k** from the compounds were determined as 0.068 ± 0.003 μm, 0.048 ± 0.002 μm, 0.027 ± 0.001 μm, 0.043 ± 0.002 μm and 0.039 ± 0.001 μm, respectively. Compound **4g** and compound **4k**, which exhibit the highest AChE activity among the 14 synthesized compounds, demonstrate that groups such as acetyl and dimethylamino propyl, substituted on the piperazine rings in their structures, interact with the CAS of the AChE enzyme. Consequently, these compounds with high activity effectively inhibit both active sites of the AChE enzyme. The compounds with long-chain, large-volume structures in the fourth position of the piperazine ring showed significant decreases in AChE enzyme inhibition values.

Compounds with similar structures were compared based on their AChE enzyme inhibition values. Compound **4a** has a one-carbon methyl group, while compound **4b** has two-carbon ethyl group. The IC$_{50}$ values of these compounds were determined as 0.068 ± 0.00 μM and 30.093 ± 0.003 μM, respectively. Considering these two compounds with similar structures, a decrease in AChE enzyme inhibition was observed when chain elongation occurs in the side groups. Similar to compounds **4a** and

Table 4 $c \log P$ and total polar surface area (TPSA) values of the synthesized compounds

Compound	AChE IC$_{50}$ (M)	MAO B IC$_{50}$ (M)	$c \log P$	TPSA
4a	0.068 ± 0.003	0.274 ± 0.012	2.48	71.11
4b	0.093 ± 0.003	>100	2.82	71.11
4c	>100	>1000	3.14	71.11
4d	>100	>1000	3.07	71.11
4e	>100	>100	2.70	71.11
4f	0.048 ± 0.002	0.137 ± 0.005	2.17	88.18
4g	0.027 ± 0.001	0.114 ± 0.003	2.32	88.18
4h	0.120 ± 0.005	>100	2.51	80.34
4i	0.084 ± 0.003	>100	2.41	91.34
4j	0.043 ± 0.002	>100	2.63	74.35
4k	0.039 ± 0.001	>1000	2.94	74.35
4l	>100	>1000	3.48	71.11
4m	0.158 ± 0.006	>100	1.97	113.63
4n	0.205 ± 0.009	>100	2.28	113.63

compound **4b**, compound **4m** features a one-carbon methyl sulfonyl structure, whereas compound **4n** incorporates a two-carbon ethyl sulfonyl structure. As observed in the previous example, chain elongation in the groups attached to the compounds negatively impacted their AChE enzyme activities.

The IC$_{50}$ values of compounds **4a**, **4f** and **4g** against the MAO B enzyme are less than 1 μM and these values are close to the reference molecule, selegiline. These compounds have IC$_{50}$ values of 0.274 ± 0.012 μM, 0.137 ± 0.005 μM, 0.114 ± 0.003 μM, respectively. Among the synthesized compounds, those featuring groups with relatively smaller spatial volumes, such as methyl, aldehyde, or acetyl, exhibited the highest activity. Conversely, compounds containing larger, long-chain groups such as isopropyl, dimethylamino propyl, methylsulfonyl, or ethylsulfonyl demonstrated a noticeable decline in activity due to their larger spatial volumes.

An examination of the $c \log P$ and TPSA data obtained from SwissADME[46] revealed a correlation between the physicochemical properties of the compounds and their biological activity (Table 4). Molecules with lower $c \log P$ values and higher TPSA values demonstrated greater efficacy, which can be seen in the higher activity of compounds **4a**, **4b**, **4f**, and **4g**, compared to the lower activity of compounds **4c**, **4d**, **4e**, and **4l**. Specifically, the compounds with higher $c \log P$ values (such as compounds **4c**, **4d**, **4e**, and **4l**) exhibited reduced biological activity, possibly due to increased lipophilicity, which might impair their interaction with biological targets. On the other hand, the compounds with higher TPSA values (such as compounds **4a**, **4b**, **4f**, and **4g**) showed increased polar surface area, which might improve solubility and interaction with polar biological targets, thereby enhancing their activity. This suggests that the balance between lipophilicity ($c \log P$) and polarity (TPSA) plays a crucial role in determining the biological activity of these compounds.

Conclusions

The ^{1}H-NMR, ^{13}C-NMR, HRMS and melting point data demonstrated a good support to the characterization of

obtained compounds. Following the characterization studies, *in vitro* and *in silico* studies were carried out. According to the *in vitro* and *in silico* studies, compound **4g** showed the highest potential activity against AChE and MAO B. The most potent derivative against AChE was **4g** with an IC$_{50}$ value of 0.027 ± 0.001 μM. Moreover, the most potent derivative against MAO B was **4g** with an IC$_{50}$ value of 0.114 ± 0.003 μM.

In molecular docking studies, compound **4g** exhibited similarities to Donepezil, but it also interacted with the amino acid Tyr133, which Donepezil does not engage with. In the dynamics study, compound **4g** formed bonds with 36 different amino acids. In interpreting these results, the continuous interactions between compound **4g** and the amino acids Trp86, Glu202, Trp286, Tyr337, Phe338 and His447, which are important for the active site of the AChE enzyme, play a significant role.

It has been observed from all of the studies that by designing, synthesizing, and evaluating the activities of synthesized compounds with similar structures in the future, it is possible to develop compounds with enhanced activity values.

Experimental

Chemistry

All the reagents are purchased from a commercial provider, and no additional purification was required before the usage. The Mettler Toledo-MP90 Melting Point System was used to determine the melting points (M.P.), without any correction. The characterization of the compounds was performed using the ^{1}H-NMR DPX 300 FT-NMR spectrometer and the ^{13}C-NMR DPX 75 MHz spectrometer (Bruker Bioscience, USA). ESI was used to record mass spectra on an LCMS-IT-TOF (Shimadzu, Kyoto, Japan). The IR spectra of the compounds were recorded using an FTIR spectrometer (Shimadzu, Japan).

The purity of the compounds was assessed by HPLC (Shimadzu, Kyoto, Japan) equipped with two LC-20AD binary pumps, a DGU-20A3R degassing unit, a CTO-10ASvp column oven, an SIL-20AC autosampler, and an SPD-M20A PDA detector. Analyses were performed on a Shim-pack FC-ODS C18 column (150 mm × 2.0 mm, 3 μm). The mobile phase consisted of acetonitrile and water (70 : 30, v/v) containing 0.1% formic acid, delivered at a flow rate of 0.25 mL min^{-1}. The injection volume was 1 μL, and the column oven temperature was maintained at 40 °C. Detection was carried out at 254 nm.

Synthesis of N-(4-(3-(3,4-dimethoxyphenyl)-3-oxoprop-1-en-1-yl)phenyl)acetamide 1

Potassium hydroxide (100 mmol, 5.6 g) was dissolved in methanol (absolute). First 3,4-dimethoxyacetophenone (100 mmol, 18.0 g) and then 4-acetamidobenzaldehyde (100 mmol, 16.3 g) were added to the solution and stirred at room temperature. After 48 hours, a colored precipitate formed and was collected by filtration. The resulting product was dried and recrystallized from ethanol.

Synthesis of 3-(4-aminophenyl)-1-(3,4-dimethoxyphenyl)prop-2-en-1-one 2

N-(4-(3-(3,4-Dimethoxyphenyl)-3-oxoprop-1-en-1-yl)phenyl) acetamide (**1**) (70 mmol, 22.75 g) was dissolved in a mixture of water (60 mL) and concentrated hydrochloric acid (37%, 20 mL). The reaction mixture was refluxed for 12 hours. Upon completion, confirmed by TLC, the mixture was cooled, ice was added, and the solution was neutralized with aqueous ammonia. The resulting precipitate was filtered, washed with water. Following these processes, the resulting product was dried and recrystallized from ethanol.

Synthesis of 2-chloro-N-(4-(3-(3,4-dimethoxyphenyl)-3-oxoprop-1-en-1-yl) phenyl) acetamide 3

In a flask, 3-(4-aminophenyl)-1-(3,4-dimethoxyphenyl)prop-2-en-1-one (**2**) (33 mmol, 9.34 g) was dissolved in THF (30 mL). Then, TEA (33 mmol, 4.63 mL) was added, and the flask was placed in an ice bath on a magnetic stirrer. Following this process, chloroacetyl chloride (33 mmol, 2.63 mL) dissolved in THF (10 mL) and was added to a dropping funnel. Subsequently, chloroacetyl chloride solution was added dropwise onto the mixing 3-(4-aminophenyl)-1-(3,4-dimethoxyphenyl) prop-2-en-1-one (**2**) solution. After the dripping process was completed, the mixture continued to be stirred for 1 hour. The completion of the reaction was confirmed by thin-layer chromatography (TLC). THF was subsequently removed from the reaction mixture, and the residue was washed with water and filtered. The crude product was then dried, followed by crystallization from ethanol.

Synthesis of the target compounds

2-Chloro-*N*-(4-(3-(3,4-dimethoxyphenyl)-3-oxoprop-1-en-1yl) phenyl)acetamide (**3**) (1 mmol, 0.36 g) and K$_2$CO$_3$ (1 mmol, 0.138 g) was taken into a flask and dissolved in acetone (30 mL) and the appropriate piperazine derivative (1 mmol) was added into the solution. Following this process, the reaction mixture was refluxed for 12 hours. After the completion of the reaction was confirmed by TLC, the mixture was transferred to an open container and acetone was removed from the environment under the fume hood. The remaining residue was then washed with water and filtered. The dried crude product was crystallized from ethanol.

N-(4-(3-(3,4-Dimethoxyphenyl)-3-oxoprop-1-en-1-yl)phenyl)-2-(4-methylpiperazin-1-yl)acetamide (4a)

Yield: 81%, TLC R_f 0.30 (petroleum ether/ethyl acetate 75 : 25, v/v), purity (HPLC): 95.5%, M.P.: 68.6 °C. FTIR (ATR, cm^{-1}): 3258 (stretching band corresponding to N–H), 1676 (stretching band corresponding to chalcone C=O), 1647 (stretching band corresponding to amide C=O), 1148 (stretching band corresponding to C–O). ^{1}H-NMR (300 MHz, DMSO-d$_6$): δ = 2.16 (3H, s, –CH$_3$), 2.37 (8H, b.s., piperazine), 3.14 (2H, s, –CH$_2$), 3.86 (3H, s, –OCH$_3$), 3.87 (3H, s, –OCH$_3$), 7.10 (1H, d, *J* = 8.59 Hz, trisubstituebenzene), 7.60 (1H, d, *J* = 1.95 Hz, Ar–H), 7.69–7.75 (3H, m, Ar–H), 7.82–7.92 (5H, m, Ar–H), 9.94 (1H, s, seconder

amine). ^{13}C-NMR (75 MHz, DMSO-d$_6$): δ = 46.24, 53.16, 54.97, 56.05, 62.31, 111.10, 111.30, 119.71, 120.66, 123.72, 130.16, 130.27, 131.08, 141.14, 143.28, 149.22, 153.57, 169.12, 187.66. HRMS (m/z): [M + H]$^+$ calcd for C$_{24}$H$_{29}$N$_3$O$_4$: 424.2231; found: 424.2239.

N-(4-(3-(3,4-Dimethoxyphenyl)-3-oxoprop-1-en-1-yl)phenyl)-2-(4-ethylpiperazin-1-yl)acetamide (4b)

Yield: 82%, TLC R_f 0.35 (petroleum ether/ethyl acetate 75 : 25, v/v), purity (HPLC): >99.9%, M.P.: 61.7 °C. FTIR (ATR, cm^{-1}): 3271 (stretching band attributed to N–H), 1678 (stretching band attributed to chalcone C=O), 1647 (stretching band attributed to amide C=O), 1147 (stretching band attributed to C–O). ^{1}H-NMR (300 MHz, DMSO-d$_6$): δ = 0.98 (3H, t, J = 7.17 Hz, –CH$_3$), 2.14–2.44 (10H, m, piperazine/–CH$_2$–), 3.13 (2H, s, –CH$_2$), 3.86 (3H, s, –OCH$_3$), 3.87 (3H, s, –OCH$_3$), 7.10 (1H, d, J = 8.56 Hz, trisubstituebenzene), 7.60 (1H, d, J = 1.93 Hz, Ar–H), 7.69–7.75 (3H, m, Ar–H), 7.82–7.91 (5H, m, Ar–H), 9.94 (1H, s, seconder amine). ^{13}C-NMR (75 MHz, DMSO-d$_6$): δ = 12.53, 52.07, 52.66, 53.31, 56.04, 56.25, 62.39, 111.05, 111.28, 119.71, 120.64, 123.71, 130.16, 130.26, 131.07, 141.15, 143.29, 149.2 0, 153.56, 169 12, 187.65. HRMS (m/z): [M + H]$^+$ calcd for C$_{25}$H$_{31}$N$_3$O$_4$: 438.2387; found: 438.2386.

N-(4-(3-(3,4-Dimethoxyphenyl)-3-oxoprop-1-en-1-yl)phenyl)-2-(4-isopropylpiperazin-1-yl)acetamide (4c)

Yield: 77%, TLC R_f 0.46 (petroleum ether/ethyl acetate 75 : 25, v/v), purity (HPLC): 96.6%, M.P.: 127.6 °C. FTIR (ATR, cm^{-1}): 3269 (stretching band attributed to N–H), 1680 (stretching band attributed to chalcone C=O), 1649 (stretching band attributed to amide C=O), 1161 (stretching band attributed to C–O). ^{1}H-NMR (300 MHz, DMSO-d$_6$): δ = 0.96 (6H, d, J = 6.51 Hz, –CH$_3$), 2.36–2.44 (4H, m, piperazine), 2.56–2.72 (5H, m, piperazine, –CH–), 3.12 (2H, s, –CH$_2$–), 3.86 (3H, s, –OCH$_3$), 3.87 (3H, s, –OCH$_3$), 7.10 (1H, d, J = 8.56 Hz, trisubstituebenzene), 7.60 (1H, d, J = 1.92 Hz, Ar–H), 7.69–7.75 (3H, m, Ar–H), 7.84–7.91 (4H, m, Ar–H), 9.92 (1H, s, seconder amine). ^{13}C-NMR (75 MHz, DMSO-d$_6$): δ = 18.73, 48.27, 53.72, 54.07, 56.05, 56.20, 62.48, 111.09, 111.29, 119.74, 120.65, 123.71, 130.16, 130.26, 131.08, 141.15, 143.29, 149.22, 153.56, 169.14, 187.65. HRMS (m/z): [M + H]$^+$ calcd for C$_{26}$H$_{33}$N$_3$O$_4$: 452.2544; found: 452.2550.

2-(4-Allylpiperazin-1-yl)-N-(4-(3-(3,4-dimethoxyphenyl)-3-oxoprop-1-en-1-yl)phenyl)acetamide (4d)

Yield: 79%, TLC R_f 0.29 (petroleum ether/ethyl acetate 75 : 25, v/v), purity (HPLC): >99.9%, M.P.: 120.8 °C. FTIR (ATR, cm^{-1}): 3265 (stretching band attributed to N–H), 1680 (stretching band attributed to chalcone C=O), 1649 (stretching band attributed to amide C=O), 1147 (stretching band attributed to C–O). ^{1}H-NMR (300 MHz, DMSO-d$_6$): δ = 2.37–2.44 (4H, m, piperazine), 2.51–2.63 (4H, m, piperazine), 2.94 (2H, d, J = 6.36 Hz, –CH$_2$–), 3.14 (2H, s, –CH$_2$–), 3.86 (3H, s, –OCH$_3$), 3.87 (3H, s, –OCH$_3$), 5.14 (2H, m, –CH$_2$–allyl), 5.80 (1H, m, –CH allyl), 7.10 (1H, d, J = 8.56 Hz, trisubstituebenzene), 7.60 (1H, d, J = 1.95 Hz, Ar–H), 7.69–7.75 (3H, m, Ar–H), 7.84–7.93 (4H, m, Ar–H), 9.93 (1H, s, seconder amine). ^{13}C-NMR (75 MHz, DMSO-d$_6$): δ = 52.85,

53.23, 56.06, 56.26, 61.33, 62.33, 111.09, 111.30, 117.91, 119.72, 120.67, 123.72, 130.16, 130.27, 131.08, 136.07, 141.14, 143.28, 149.22, 153.57, 169.10, 187.65. HRMS (m/z): [M + H]$^+$ calcd for C$_{26}$H$_{31}$N$_3$O$_4$: 450.2387; found: 450.2388.

N-(4-(3-(3,4-Dimethoxyphenyl)-3-oxoprop-1-en-1-yl)phenyl)-2-(4-(prop-2-yn-1-yl)piperazin-1-yl)acetamide (4e)

Yield: 78%, TLC R_f 0.26 (petroleum ether/ethyl acetate 75 : 25, v/v), purity (HPLC): >99.9%, M.P.: 74.5 °C. FTIR (ATR, cm^{-1}): 3261 (stretching band attributed to N–H), 1676 (stretching band attributed to chalcone C=O), 1647 (stretching band attributed to amide C=O), 1149 (stretching band attributed to C–O). ^{1}H-NMR (300 MHz, DMSO-d$_6$): δ = 2.37–2.49 (4H, m, piperazine), 2.52–2.59 (4H, m, piperazine), 3.15 (2H, s, –CH$_2$–), 3.17 (1H, s, –CH), 3.26 (2H, s, –CH$_2$–), 3.86 (3H, s, –OCH$_3$), 3.87 (3H, s, –OCH$_3$), 7.10 (1H, d, J = 8.56 Hz, trisubstituebenzene), 7.60 (1H, d, J = 1.95 Hz, Ar–H), 7.69–7.75 (3H, m, Ar–H), 7.84–7.92 (4H, m, Ar–H), 9.96 (1H, s, seconder amine). ^{13}C-NMR (75 MHz, DMSO-d$_6$): δ = 46.45, 51.47, 53.07, 56.06, 56.20, 62.31, 76.18, 79.94, 111.08, 111.30, 119.75, 120.67, 123.71, 130.15, 130.26, 131.08, 141.18, 143.29, 149.22, 153.57, 169.08, 187.66. HRMS (m/z): [M + H]$^+$ calcd for C$_{26}$H$_{29}$N$_3$O$_4$: 448.2231; found: 448.2248.

N-(4-(3-(3,4-Dimethoxyphenyl)-3-oxoprop-1-en-1-yl)phenyl)-2-(4-formylpiperazin-1-yl)acetamide (4f)

Yield: 73%, TLC R_f 0.40 (petroleum ether/ethyl acetate 75 : 25, v/v), purity (HPLC): 97.6%, M.P.: 104.1 °C. FTIR (ATR, cm^{-1}): 3277 (stretching band attributed to N–H), 1651 (stretching band attributed to chalcone C=O), 1573 (stretching band attributed to amide C=O), 1146 (stretching band attributed to C–O). ^{1}H-NMR (300 MHz, DMSO-d$_6$): δ = 2.37–2.49 (2H, m, piperazine), 2.53–2.63 (2H, m, piperazine), 3.22 (2H, s, –CH$_2$–), 3.41–3.54 (4H, m, piperazine), 3.86 (3H, s, –OCH$_3$), 3.87 (3H, s, –OCH$_3$), 7.10 (1H, d, J = 8.55 Hz, trisubstituebenzene), 7.60 (1H, d, J = 1.91 Hz, Ar–H), 7.70–7.77 (3H, m, Ar–H), 7.85–7.92 (4H, m, Ar–H), 8.01 (1H, s, –CH–), 10.02 (1H, s, seconder amine). ^{13}C-NMR (75 MHz, DMSO-d$_6$): δ = 44.09, 45.13, 52.44, 53.59, 56.04, 56.193 61.87, 111.05, 111.28, 119.80, 120.67, 123.73, 130.16, 130.31, 131.06, 141.13, 143.28, 149.21, 153.56, 161.23, 165.39, 168.95, 187.64. HRMS (m/z): [M + H]$^+$ calcd for C$_{24}$H$_{27}$N$_3$O$_5$: 438.2023; found: 438.2043.

2-(4-Acetylpiperazin-1-yl)-N-(4-(3-(3,4-dimethoxyphenyl)-3-oxoprop-1-en-1-yl)phenyl)acetamide (4g)

Yield: 82%, TLC R_f 0.25 (petroleum ether/ethyl acetate 75 : 25, v/v), purity (HPLC): 95.3%, M.P.: 81.8 °C. FTIR (ATR, cm^{-1}): 3279 (stretching band attributed to N–H), 1620 (stretching band attributed to chalcone C=O), 1562 (stretching band attributed to amide C=O), 1139 (stretching band attributed to C–O). ^{1}H-NMR (300 MHz, DMSO-d$_6$): δ = 1.99 (3H, s, –CH$_3$), 2.45–2.49 (2H, m, piperazine), 2.51–2.57 (2H, m, piperazine), 3.20 (2H, s, –CH$_2$–), 3.47–3.55 (4H, b.s., piperazine), 3.86 (3H, s, –OCH$_3$), 3.87 (3H, s, –OCH$_3$), 7.10 (1H, d, J = 8.57 Hz, trisubstituebenzene), 7.60 (1H, d, J = 1.89 Hz, Ar–H), 7.70–7.76 (3H, m, Ar–H), 7.85 (4H, m, Ar–H), 10.02 (1H, s, seconder amine). ^{13}C-NMR (75 MHz, DMSO-d$_6$): δ = 21.69, 46.01, 52.82, 56.04, 56.19, 61.92,

111.06, 111.28, 119.78, 120.66, 123.72, 130.16, 130.30, 131.06, 141.14, 143.28, 149.21, 153.56, 168.62, 168.99, 187.64. HRMS (m/z): $[M + H]^+$ calcd for $C_{25}H_{29}N_3O_5$: 452.2180; found: 452.2192.

N-(4-(3-(3,4-Dimethoxyphenyl)-3-oxoprop-1-en-1-yl)phenyl)-2-(4-(2-methoxyethyl)piperazin-1-yl)acetamide (4h)

Yield: 77%, TLC R_f 0.23 (petroleum ether/ethyl acetate 75 : 25, v/v), purity (HPLC): >99.9%, M.P.: 53.5 °C. FTIR (ATR, cm^{-1}): 3265 (stretching band attributed to N–H), 1676 (stretching band attributed to chalcone C=O), 1645 (stretching band attributed to amide C=O), 1148 (stretching band attributed to C–O). ^{1}H-NMR (300 MHz, DMSO-d$_6$): δ = 2.38–2.49 (8H, m, piperazine), 3.14 (2H, d, J = 7.90 Hz, –CH$_2$–), 3.22 (2H, s, –CH$_2$–), 3.29 (2H, d, J = 4.95 Hz, –CH$_2$–), 3.42 (3H, m, –CH$_3$), 3.86 (3H, s, –OCH$_3$), 3.87 (3H, s, –OCH$_3$), 7.10 (1H, d, J = 8.56 Hz, trisubstituebenzene), 7.60 (1H, d, J = 1.95 Hz, Ar–H), 7.69–7.75 (3H, m, Ar–H), 7.84–7.92 (4H, m, Ar–H), 9.94 (1H, s, seconder amine). ^{13}C-NMR (75 MHz, DMSO-d$_6$): δ = 53.28, 53.43, 56.05, 56.26, 57.51, 58.46, 62.36, 70.39, 111.09, 111.29, 119.72, 120.66, 123.73, 130.17, 130.26, 131.08, 141.15, 143.29, 149.22, 153.56, 169.12, 187.66. HRMS (m/z): $[M + H]^+$ calcd for $C_{26}H_{33}N_3O_5$: 468.2493; found: 468.2500.

N-(4-(3-(3,4-Dimethoxyphenyl)-3-oxoprop-1-en-1-yl)phenyl)-2-(4-(3-hydroxypropyl)piperazin-1-yl)acetamide (4i)

Yield: 78%, TLC R_f 0.48 (petroleum ether/ethyl acetate 75 : 25, v/v), purity (HPLC): 97.1%, M.P.: 152.9 °C. FTIR (ATR, cm^{-1}): 3287 (stretching band attributed to N–H), 1688 (stretching band attributed to chalcone C=O), 1651 (stretching band attributed to amide C=O), 1150 (stretching band attributed to C–O). ^{1}H-NMR (300 MHz, DMSO-d$_6$): δ = 1.56 (2H, m, –CH$_2$–), 2.20–2.49 (10H, m, piperazine, –CH$_2$–), 2.64 (1H, m, CH), 3.14 (2H, s, –CH$_2$–), 3.44 (2H, d, J = 6.25 Hz, –CH$_2$–), 3.86 (3H, s, –OCH$_3$), 3.87 (3H, s, –OCH$_3$), 4.49 (1H, b.s., –OH), 7.10 (1H, d, J = 8.57 Hz, trisubstituebenzene), 7.60 (1H, d, J = 1.92 Hz, Ar–H), 7.69 (1H, s, trisubstituebenzene), 7.74 (2H, d, J = 8.74 Hz, disubstituebenzene), 7.84 (2H, d, J = 3.22 Hz, disubstitutedbenzene), 7.88 (1H, m, trisubstituebenzene), 7.91 (1H, m, Ar–H), 9.94 (1H, s, seconder amine). ^{13}C-NMR (75 MHz, DMSO-d$_6$): δ = 30.03, 53.14, 53.32, 55.60, 56.04, 59.90, 62.35, 111.05, 111.28, 119.71, 120.64, 123.72, 130.17, 130.26, 131.07, 141.15, 143.29, 149.21, 153.55, 169.12, 187.64. HRMS (m/z): $[M + H]^+$ calcd for $C_{26}H_{33}N_3O_5$: 468.2493; found: 468.2503.

N-(4-(3-(3,4-Dimethoxyphenyl)-3-oxoprop-1-en-1-yl)phenyl)-2-(4-(2-(dimethylamino)ethyl)piperazin-1-yl)acetamide (4j)

Yield: 78%, TLC R_f 0.30 (petroleum ether/ethyl acetate 75 : 25, v/v), purity (HPLC): >99.9%, M.P.: 152.9 °C. FTIR (ATR, cm^{-1}): 3289 (stretching band attributed to N–H), 1682 (stretching band attributed to chalcone C=O), 1647 (stretching band attributed to amide C=O), 1152 (stretching band attributed to C–O). ^{1}H-NMR (300 MHz, DMSO-d$_6$): δ = 2.11 (6H, s, dimethylamino), 2.24–2.41 (8H, m, piperazine), 2.44–2.45 (4H, m, –CH$_2$CH$_2$–), 3.13 (2H, s, –CH$_2$), 3.86 (3H, s, –OCH$_3$), 3.87 (3H, s, –OCH$_3$), 7.10 (1H, d, J = 8.59 Hz, trisubstituebenzene), 7.60 (1H, d, J = 1.98 Hz, Ar–H), 7.69–7.75 (3H, m, Ar–H), 7.83–7.92 (4H, m, Ar–

H), 9.99 (1H, s, seconder amine). ^{13}C-NMR (75 MHz, DMSO-d$_6$): δ = 46.02, 53.30, 53.40, 56.05, 56.25, 56.40, 57.12, 62.35, 111.09, 111.29, 119.71, 120.64, 123.71, 130.15, 130.24, 131.08, 141.18, 143.29, 149.22, 153.56, 169.12, 187.65. HRMS (m/z): $[M + H]^+$ calcd for $C_{27}H_{36}N_4O_4$: 468.2493; found: 468.2503.

N-(4-(3-(3,4-Dimethoxyphenyl)-3-oxoprop-1-en-1-yl)phenyl)-2-(4-(3-(dimethylamino)propyl)piperazin-1-yl)acetamide (4k)

Yield: 80%, TLC R_f 0.39 (petroleum ether/ethyl acetate 75 : 25, v/v), purity (HPLC): >99.9%, M.P.: 129.3 °C. FTIR (ATR, cm^{-1}): 3291 (stretching band attributed to N–H), 1682 (stretching band attributed to chalcone C=O), 1649 (stretching band attributed to amide C=O), 1152 (stretching band attributed to C–O). ^{1}H-NMR (300 MHz, DMSO-d$_6$): δ = 1.51 (2H, m, –CH$_2$–), 2.08 (6H, s, dimetilamino), 2.18 (2H, d, J = 7.17 Hz, –CH$_2$–), 2.24 (2H, d, J = 7.35 Hz, –CH$_2$–) 2.40 (8H, b.s., piperazine), 3.14 (2H, s, –CH$_2$–), 3.86 (3H, s, –OCH$_3$), 3.87 (3H, s, –OCH$_3$), 7.10 (1H, d, J = 8.59 Hz, trisubstituebenzene), 7.60 (1H, d, J = 1.86 Hz, Ar–H), 7.69–7.76 (3H, m, Ar–H), 7.83–7.92 (4H, m, Ar–H), 10.02 (1H, s, seconder amine). ^{13}C-NMR (75 MHz, DMSO-d$_6$): δ = 25.03, 45.67, 53.13, 53.30, 56.04, 56.24, 56.47, 57.77, 62.34, 111.06, 111.27, 119.71, 120.62, 123.71, 130.15, 130.23, 131.08, 141.20, 143.30, 149.21, 153.55, 169.13, 187.64. HRMS (m/z): $[M + H]^+$ calcd for $C_{28}H_{38}N_4O_4$: 248.1519; found: 248.1513.

2-(4-Cyclopentylpiperazin-1-yl)-N-(4-(3-(3,4-dimethoxyphenyl)-3-oxoprop-1-en-1-yl)phenyl)acetamide (4l)

Yield: 78%, TLC R_f 0.31 (petroleum ether/ethyl acetate 75 : 25, v/v), purity (HPLC): >99.9%, M.P.: 72.8 °C. FTIR (ATR, cm^{-1}): 3265 (stretching band attributed to N–H), 1694 (stretching band attributed to chalcone C=O), 1657 (stretching band attributed to amide C=O), 1163 (stretching band attributed to C–O). ^{1}H-NMR (300 MHz, DMSO-d$_6$): δ = 1.25–1.32 (2H, m, cyclopentyl), 1.45–.1.50 (2H, m, cyclopentyl), 1.52–1.58 (2H, m, cyclopentyl), 1.71–1.78 (2H, m, cyclopentyl), 2.33–2.49 (8H, m, piperazine), 2.55–2.57 (1H, m, cyclopentyl), 3.12 (2H, s, –CH$_2$–), 3.86 (3H, s, –OCH$_3$), 3.87 (3H, s, –OCH$_3$), 7.10 (1H, d, J = 8.59 Hz, trisubstituebenzene), 7.60 (1H, d, J = 1.98 Hz, Ar–H), 7.69–7.76 (3H, m, Ar–H), 7.84–7.92 (4H, m, Ar–H), 9.98 (1H, s, seconder amine). ^{13}C-NMR (75 MHz, DMSO-d$_6$): δ = 24.11, 30.43, 51.98, 53.39, 56.04, 56.25, 62.40, 67.17, 111.08, 111.28, 119.71, 120.62, 123.72, 130.16, 130.24, 131.07, 141.19, 143.29, 149.21, 153.55, 169.12, 187.64. HRMS (m/z): $[M + H]^+$ calcd for $C_{28}H_{35}N_3O_4$: 478.2700; found: 478.2718.

N-(4-(3-(3,4-Dimethoxyphenyl)-3-oxoprop-1-en-1-yl)phenyl)-2-(4-(methylsulfonyl)piperazin-1-yl)acetamide (4m)

Yield: 79%, TLC R_f 0.33 (petroleum ether/ethyl acetate 75 : 25, v/v), purity (HPLC): >99.9%, M.P.: 112.6 °C. FTIR (ATR, cm^{-1}): 3308 (stretching band attributed to N–H), 1682 (stretching band attributed to chalcone C=O), 1651 (stretching band attributed to amide C=O), 1157 (stretching band attributed to C–O). ^{1}H-NMR (300 MHz, DMSO-d$_6$): δ = 2.62–2.65 (4H, m, piperazine), 2.82 (2H, s, –CH$_2$–), 2.90 (3H, s, –CH$_3$), 3.16–3.19 (4H, m, piperazine), 3.86 (3H, s, –OCH$_3$), 3.87 (3H, s, –OCH$_3$), 7.10 (1H, d, J = 8.57 Hz, trisubstituebenzene), 7.60 (1H, d, J = 1.89 Hz, Ar–

H), 7.69–7.76 (3H, m, Ar–H), 7.83–7.92 (4H, m, Ar–H), 10.04 (1H, s, seconder amine). ^{13}C-NMR (75 MHz, DMSO-d$_6$): $\delta =$ 34.20, 45.77, 52.30, 56.05, 56.26, 61.53, 111.07, 111.29, 119.77, 120.69, 123.74, 130.16, 130.31, 131.07, 141.15, 143.27, 149.22, 153.57, 168.90, 187.65. HRMS (m/z): [M + H]$^+$ calcd for C$_{24}$H$_{29}$N$_3$O$_6$S: 488.1850; found: 488.1855.

N-(4-(3-(3,4-Imethoxyphenyl)-3-oxoprop-1-en-1-yl)phenyl)-2-(4-(ethylsulfonyl)piperazin-1-yl)acetamide (4n)

Yield: 80%, TLC R_f 0.43 (petroleum ether/ethyl acetate 75 : 25, v/v), purity (HPLC): >99.9%, M.P.: 100.9 °C. FTIR (ATR, cm^{-1}): 3298 (stretching band attributed to N–H), 1682 (stretching band attributed to chalcone C=O), 1655 (stretching band attributed to amide C=O), 1150 (stretching band attributed to C–O). ^{1}H-NMR (300 MHz, DMSO-d$_6$): $\delta =$ 1.20–1.25 (3H, m, –CH$_3$), 2.59–2.72 (4H, m, piperazine), 3.05–3.11 (2H, m, –CH$_2$–), 3.17 (2H, s, –CH$_2$–), 3.24 (4H, b.s., piperazine), 3.86 (3H, s, –OCH$_3$), 3.87 (3H, s, –OCH$_3$), 7.10 (1H, d, J = 8.59 Hz, tri-substituebenzene), 7.60 (1H, d, J = 1.95 Hz, Ar–H), 7.69–7.76 (3H, m, Ar–H), 7.85–7.92 (4H, m, Ar–H), 10.05 (1H, s, seconder amine). ^{13}C-NMR (75 MHz, DMSO-d$_6$): $\delta =$ 7.95, 42.78, 45.59, 52.65, 56.05, 56.26, 61.59, 111.07, 111.29, 119.79, 120.67, 123.72, 130.16, 130.30, 131.06, 141.15, 143.28, 149.21, 153.56, 168.93, 187.64. HRMS (m/z): [M + H]$^+$ calcd for C$_{25}$H$_{31}$N$_3$O$_6$S: 502.2006; found: 502.2022.

Anticholinesterase enzyme activity studies

Anticholinesterase enzyme activity studies were conducted by investigating the enzyme inhibition properties of compounds obtained through a modified version of the colorimetric Ellman method. Prior to initiating the inhibition studies, all solutions were equilibrated to a temperature of 20–25 °C. During the experiments, 96-well microplates were utilized. Each well was brought to a final volume of 210 µL using two different test solutions.

The first test solution consisted of 20 µL enzyme solution, 20 µL DTNB solution, and 70 µL phosphate buffer per well. The second test solution included 10 µL ATC/BTC and 70 µL phosphate buffer per well. Upon addition of the enzyme inhibitors, the final composition per well was as follows: 10 µL ATC/BTC, 20 µL enzyme solution, 20 µL inhibitor solution, 20 µL DTNB solution, and 140 µL phosphate buffer, bringing the total volume to 210 µL in each well.

Initially, 110 µL of the first test solution and 20 µL of inhibitor solutions at varying concentrations were transferred into the wells of 96-well plates using the Biotek Precision XS (USA) robotic system. Inhibitor compounds were applied in quadruplicate for each concentration. The prepared plates were then placed in a BioTek-Synergy H1 (USA) microplate reader, where they underwent a 5-minute mixing step followed by a 15-minute incubation period at 25 °C.

At the end of the 15-minute incubation, 80 µL of the second test solution, stored in the dispenser compartment of the microplate reader, was added to each well. After the addition of the second test solution, a 30-second mixing step was performed. Subsequently, the first absorbance reading was

recorded at a wavelength of 412 nm. To allow the reaction to proceed, an additional 5-minute mixing step was carried out, followed by the second absorbance measurement.[37,47,48]

Blank, control and all concentrations of inhibitors were analyzed in quadruplicate. The percentage of inhibition results were displayed as the mean ± standard deviation (SD). Moreover, the IC$_{50}$ values were calculated with the help of *GraphPad 'PRISM'* software (version 5.0) by using a dose–response curve achieved by plotting the percentage inhibition *versus* the log concentration.

The percent inhibition values were calculated using the differences between the two absorbance readings obtained during the assay, as shown in equation:

$$\% \text{ inhibition} = [(A(C) - A(B)) - (A(I) - A(B))]/((A(C) - A(B))) \times 100$$

where: B (Blank): well containing neither inhibitor compound nor substrate, C (Control): well containing only the enzyme without inhibitor, A(B): absorbance difference of the blank well, A(C): absorbance difference of the control well, A(I): absorbance difference of the inhibitor-containing well.

Monoamine oxidase enzyme activity studies

The inhibitory activities of the synthesized compounds against MAO A and MAO B enzymes were determined using a fluorometric method. For the MAO enzyme inhibition assays, three different solutions were freshly prepared on the day of the experiment.

The first solution consisted of inhibitor solutions prepared at various concentrations of the synthesized compounds and reference drug compounds. The second solution included the enzyme solutions. To prepare these, hMAO A (0.5 U mL^{-1}) and recombinant hMAO B (0.64 U mL^{-1}) enzymes were dissolved in phosphate buffer, and the total volume was adjusted to 10 mL.

Finally, the working solution was prepared by dissolving horseradish peroxidase (200 U mL^{-1}, 100 µL), tyramine (100 mM, 200 µL), and Ampliflu™ Red (20 mM, 200 µL) in phosphate buffer, and the final volume was adjusted to 10 mL.

Into each well of a black, flat-bottomed 96-well microplate, 20 µL of inhibitor solution and 100 µL of either of the enzyme solutions were added. The plate was then incubated for 30 minutes at 37 °C. Following this incubation step, 100 µL of the working solution was added to initiate the reaction. Subsequently, a second incubation was carried out for another 30 minutes at 37 °C, during which fluorescence measurements (E_x/E_m = 535/587 nm) were taken every 5 minutes.

For the control experiment, 2% DMSO solution was used instead of the inhibitor solution. To evaluate any inhibitory effects of the compounds on horseradish peroxidase, a parallel set of readings was taken in which 3% H$_2$O$_2$ (20 mM) solution was used instead of the enzyme solutions, allowing for the monitoring of potential inhibition toward horseradish peroxidase.[47,48]

All measurements—including blanks, controls, and each concentration of the inhibitors—were performed in

quadruplicate. The percent inhibition values were calculated using equation below:

$$\% \text{ inhibition} = [(FCt_2 - FCt_1) - (FIt_2 - FIt_1)]/(FCt_2 - FCt_1) \times 100$$

where: FCt_2: fluorescence value of the control at time point t_2, FCt_1: fluorescence value of the control at time point t_1, FIt_2: fluorescence value of the inhibitor at time point t_2, FIt_1: fluorescence value of the inhibitor at time point t_1.

The IC_{50} values of the synthesized compounds were calculated using Microsoft Office Excel 2013. Nonlinear regression analysis with a sigmoidal dose–response model was applied, and inhibition curves were plotted to determine the IC_{50} values. Blank, control and all concentrations of inhibitors were analyzed in quadruplicate. The percentage of inhibition results were displayed as the mean ± standard deviation (SD). Moreover, the IC_{50} values were calculated with the help of *GraphPad 'PRISM'* software (version 5.0) by using a dose–response curve achieved by plotting the percentage inhibition *versus* the log concentration.

Kinetic studies of AChE enzyme snhibition

The compound **4g**, which was found to be the most effective derivative in the series, was included in the enzyme kinetics study to assign the type of inhibition. For this purpose, this compound was prepared at different concentrations (IC_{50}, 2 × IC_{50} and $IC_{50}/2$). Moreover, a substrate (ATC) was used at various concentrations (600, 300, 150, 75, 37.5, and 18.75 μM). The enzyme kinetics assay was carried out as in our previous publications.[37–39] Lineweaver–Burk plots were formed using Microsoft Office Excel 2013. The K_i values of the compound were easily calculated from the second plot with a common intercept on the *x*-axis (corresponding to $-K_i$).

Cytotoxicity assay

The reduction of the colorless 3-(4,5-dimethylthiazol-2-yl)-2,5 diphenyltetrazolium salt to the purple-colored formazan product provides the basis for the MTT test, which is used to assess the metabolic activity of live cells. This color shift allows for the spectroscopic determination of the cell viability rate. A 24-hour MTT assay was conducted with a healthy cell line (NIH3T3). The NIH3T3 cells were seeded at a density of 1×10^6 cells into the 96-well plates.[37,47,49]

Molecular docking

A structure-based *in silico* docking method was used to identify potential interactions and binding sites between the **4g** labeled molecule which emerged as the most potent compound against AChE, BChE, and MAO B enzymes in this investigation. In this study, an investigation of protein–ligand interactions was conducted using the crystal structure of PDB: 4EY7 (ref. 16) for the AChE enzyme. Initially, the Schrödinger Suite 2015 Update 2 "Protein Preparation Wizard" contained the crystal structure.[50] The crystal structure was prepared for docking investigations following a specific protocol. The potential charges of the atoms on the charged amino acids under the given environmental conditions were automatically calculated, and bond lengths were adjusted using the OPLS 2005 force field. Compounds for molecular docking studies were prepared using the LigPrep 3.8 module[51] The grid was generated with Glide 7.1 (ref. 52), which was also used to conduct docking studies with single precision (SP).

Molecular dynamics simulation

In this study, the compound **4g** was subjected to molecular dynamics (MD) simulations, which are regarded as a crucial computational technique for assessing the time-dependent stability of a ligand in an active site for a drug–receptor complex.[53] 100 ns of MD simulations were run to confirm the stability of the complexes identified from the docking result. The Desmond implementation[54] was used for dynamic research. It started with a 3-point (TIP3P) water model and proceeded to apply the standard force field of the Schrödinger Suite (OPLS3e) with a transferable intermolecular potential and complex energy minimization. By employing Na and Cl ions to guarantee system neutralization and replicate the physiological concentration of monovalent ions, it yields a final salt concentration of 0.15 M.[55] The ensemble used was constant number of particles, pressure, and temperature (NPT), with a constant temperature of 310.55 K and pressure of 1.01325 bar. The equations of motion were integrated using the RESPA integrator.[56] The pressure was controlled using the MTK method[57] and the simulation temperature was maintained at a consistent level using NH thermostats.[58] The pmE approach was utilized to calculate electrostatic interactions across long distances.[59] 9.0 Å was selected for van der Waals and short-range electrostatic interactions. The standard technique offered by Desmond, which includes a sequence of restricted minimization and molecular dynamics simulations used to gradually relax the system, was employed to achieve system equilibrium. Once the system setup was completed, the MD simulation was executed using the previously mentioned parameters. The Desmond application was used to calculate the values of Rg (radius of gyration), RMSF (root mean square fluctuation), and RMSD (root mean square deviation).[54]

Molecular dynamics (MD) simulations were performed with the Desmond package (Schrödinger, LLC). The protein–ligand complex was embedded in an orthorhombic box solvated with TIP3P water molecules, resulting in a system of 63 943 atoms including 13 698 waters. Counter-ions (47 Na$^+$ and 38 Cl$^-$) were added to neutralize the system at 0.15 M ionic strength. Energy minimization was followed by equilibration with positional restraints on the protein heavy atoms. The production run was performed for 100 ns at 310 K and 1 bar using the NPgT ensemble. The integration time step was 2 fs. Long-range electrostatic interactions were treated with the particle mesh Ewald (PME) method with a 9 Å cutoff.

Trajectory analyses, including root mean square deviation (RMSD) and root mean square fluctuation (RMSF), were carried out using the Simulation Event Analysis module in Maestro.

Since only a single trajectory was performed due to computational limitations, error shading could not be provided.

Author contributions

Berkant Kurban: conceptualization, methodology, data curation. Begüm Nurpelin Sağlık Özkan: software, methodology, validation, writing—original draft preparation. Derya Osmaniye: conceptualization, methodology, software, validation, formal analysis, investigation, resources, data curation, writing—original draft preparation, visualization. Serkan Levent: methodology, formal analysis, writing—original draft preparation. Yusuf Özkay: resources, writing – review and editing, supervision. Zafer Asım Kaplancıklı: conceptualization, investigation, resources, writing – orginal draft preparation, visualization, supervision.

Conflicts of interest

There are no conflicts to declare.

Data availability

The data supporting this article have been included as part of the supplementary information (SI). Supplementary information: FTIR, ^{1}H-NMR, ^{13}C-NMR, and HRMS spectra, along with HPLC chromatograms. See DOI: https://doi.org/10.1039/d5ra05397h.

Acknowledgements

References

1 J. A. Soria Lopez, H. M. González and G. C. Léger, in *Handbook of Clinical Neurology*, ed. S. T. Dekosky and S. Asthana, Elsevier, 2019, vol. 167, pp. 231–255.

2 F. B. Ahmad and R. N. Anderson, *JAMA*, 2021, **325**(18), DOI: 10.1001/jama.2021.5469.

3 World Health Organization, *Global status report on the public health response to dementia*, 2021.

4 *Alzheimer's Dementia*, 2022, **18**, 700–789, DOI: 10.1002/alz.12638.

5 Y. Bayraktar, E. Isik, I. Isik, A. Ozyilmaz, M. Toprak, F. K. Guloglu and S. Aydin, *Sustainability*, 2022, **14**(13), 7901.

6 J. W. Kinney, S. M. Bemiller, A. S. Murtishaw, A. M. Leisgang, A. M. Salazar and B. T. Lamb, *Alzheimer's Dementia*, 2018, DOI: 10.1016/j.trci.2018.06.014.

7 P. Scheltens, K. Blennow, M. M. B. Breteler, B. de Strooper, G. B. Frisoni, S. Salloway and W. M. Van der Flier, *Lancet*, 2016, **388**, 505–517.

8 D. J. Selkoe and J. Hardy, *EMBO Mol Med*, 2016, **8**, 595–608.

9 T. Thomas, *Neurobiol. Aging*, 2000, **21**(2), 343–348.

10 G. Livingston, A. Sommerlad, V. Orgeta, S. G. Costafreda, J. Huntley, D. Ames, C. Ballard, S. Banerjee, A. Burns, J. Cohen-Mansfield, C. Cooper, N. Fox, L. N. Gitlin, R. Howard, H. C. Kales, E. B. Larson, K. Ritchie, K. Rockwood, E. L. Sampson, Q. Samus, L. S. Schneider, G. Selbæk, L. Teri and N. Mukadam, *Lancet*, 2017, **390**, 2673–2734.

11 R. T. Bartus, R. L. Dean, B. Beer and A. S. Lippa, *Science*, 1982, **217**, 408–414.

12 L. A. Craig, N. S. Hong and R. J. McDonald, *Neurosci. Biobehav. Rev.*, 2011, **35**, 1397–1409.

13 H. Hampel, M.-M. Mesulam, A. C. Cuello, M. R. Farlow, E. Giacobini, G. T. Grossberg, A. S. Khachaturian, A. Vergallo, E. Cavedo, P. J. Snyder and Z. S. Khachaturian, *Brain*, 2018, **141**, 1917–1933.

14 M. Pohanka, *Biomed. Pap.*, 2011, **155**, 219–230.

15 P. Anand and B. Singh, *Arch. Pharmacal Res.*, 2013, **36**, 375–399.

16 J. Cheung, M. J. Rudolph, F. Burshteyn, M. S. Cassidy, E. N. Gary, J. Love, M. C. Franklin and J. J. Height, *J. Med. Chem.*, 2012, **55**, 10282–10286.

17 Ł. J. Walczak-Nowicka and M. Herbet, *Int. J. Mol. Sci.*, 2021, **22**(17), 9290.

18 H. Soreq and S. Seidman, *Nat. Rev. Neurosci.*, 2001, **2**, 294–302.

19 N. H. Greig, T. Utsuki, D. K. Ingram, Y. Wang, G. Pepeu, C. Scali, Q.-S. Yu, J. Mamczarz, H. W. Holloway, T. Giordano, D. Chen, K. Furukawa, K. Sambamurti, A. Brossi and D. K. Lahiri, *Proc. Natl. Acad. Sci. U. S. A.*, 2005, **102**, 17213–17218.

20 M. B. Čolović, D. Z. Krstić, T. D. Lazarević-Pašti, A. M. Bondžić and V. M. Vasić, *Curr. Neuropharmacol.*, 2013, **11**, 315–335.

21 R. C. Petersen, R. G. Thomas, M. Grundman, D. Bennett, R. Doody, S. Ferris, D. Galasko, S. Jin, J. Kaye, A. Levey, E. Pfeiffer, M. Sano, C. H. van Dyck and L. J. Thal, *N. Engl. J. Med.*, 2005, **352**, 2379–2388.

22 M. Naoi, W. Maruyama, K. Inaba-Hasegawa and Y. Akao, in *International Review of Neurobiology*, Academic Press Inc., 2011, vol. 100, pp. 85–106.

23 M. B. H. Youdim, D. Edmondson and K. F. Tipton, *Nat. Rev. Neurosci.*, 2006, **7**, 295–309.

24 F. Chimenti, R. Fioravanti, A. Bolasco, P. Chimenti, D. Secci, F. Rossi, M. Yáñez, F. Orallo, F. Ortuso and S. Alcaro, *J. Med. Chem.*, 2009, **52**, 2818–2824.

25 J. P. M. Finberg and J. M. Rabey, *Front. Pharmacol.*, 2016, **7**, DOI: 10.3389/fphar.2016.00340.

26 Z. Fišar, *Prog. Neuropsychopharmacol. Biol. Psychiatry*, 2016, **69**, 112–124.

27 R. Cacabelos, *Int. J. Mol. Sci.*, 2017, **18**(3), 551.

28 R. E. González-Reyes, M. O. Nava-Mesa, K. Vargas-Sánchez, D. Ariza-Salamanca and L. Mora-Muñoz, *Front. Mol. Neurosci.*, 2017, **10**, DOI: 10.3389/fnmol.2017.00427.

29 M. S. Uddin, M. T. Kabir, M. M. Rahman, B. Mathew, M. A. Shah and G. M. Ashraf, *J. Pharm. Pharmacol.*, 2020, **72**, 1001–1012.

30 M. Unzeta, G. Esteban, I. Bolea, W. A. Fogel, R. R. Ramsay, M. B. H. Youdim, K. F. Tipton and J. Marco-Contelles, *Front Neurosci*, 2016, **10**, DOI: **10.3389/fnins.2016.00205**.

31 S.-S. Xie, X. Wang, N. Jiang, W. Yu, K. D. G. Wang, J.-S. Lan, Z.-R. Li and L.-Y. Kong, *Eur. J. Med. Chem.*, 2015, **95**, 153–165.

32 B. Mathew, J. M. Oh, R. S. Baty, G. E.-S. Batiha, D. G. T. Parambi, N. Gambacorta, O. Nicolotti and H. Kim, *Environ. Sci. Pollut. Res.*, 2021, **28**, 38855–38866.

33 S. Carradori and R. Silvestri, *Am. Chem. Soc.*, 2015, **58**(17), 6717–6732.

34 A. Mallia and J. Sloop, *Molecules*, 2023, **28**(7), DOI: **10.3390/molecules28073201**.

35 Z. Sang, P. Bai, Y. Ban, K. Wang, A. Wu, J. Mi, J. Hu, R. Xu, G. Zhu, J. Wang, J. Zhang, C. Wang, Z. Tan and L. Tang, *Bioorg. Chem.*, 2022, **127**, 106007.

36 U. Acar Çevik, B. N. Sağlık, D. Osmaniye, S. Levent, B. Kaya Çavuşoğlu, A. B. Karaduman, Ö. Atlı Eklioğlu, Y. Özkay and Z. A. Kaplancıklı, *J. Enzyme Inhib. Med. Chem.*, 2020, **35**, 1657–1673.

37 B. N. Sağlık, S. Ilgın and Y. Özkay, *Eur. J. Med. Chem.*, 2016, **124**, 1026–1040.

38 Ü. Demir Özkay, Ö. D. Can, B. N. Sağlık, U. Acar Çevik, S. Levent, Y. Özkay, S. Ilgın and Ö. Atlı, *Bioorg. Med. Chem. Lett.*, 2016, **26**, 5387–5394.

39 F. Tok, B. Koçyiğit-Kaymakçıoğlu, B. N. Sağlık, S. Levent, Y. Özkay and Z. A. Kaplancıklı, *Bioorg. Chem.*, 2019, **84**, 41–50.

40 M. Atanasova, G. Stavrakov, I. Philipova, D. Zheleva, N. Yordanov and I. Doytchinova, *Bioorg. Med. Chem.*, 2015, **23**, 5382–5389.

41 H. Dvir, I. Silman, M. Harel, T. L. Rosenberry and J. L. Sussman, *Chem. Biol. Interact.*, 2010, **187**, 10–22.

42 M.-Y. Wu, G. Esteban, S. Brogi, M. Shionoya, L. Wang, G. Campiani, M. Unzeta, T. Inokuchi, S. Butini and J. Marco-Contelles, *Eur. J. Med. Chem.*, 2016, **121**, 864–879.

43 B. Mathew, D. G. T. Parambi, G. E. Mathew, Md. S. Uddin, S. T. Inasu, H. Kim, A. Marathakam, M. K. Unnikrishnan and S. Carradori, *Arch. Pharm.*, 2019, **352**, 1900177.

44 P. Costanzo, L. Cariati, D. Desiderio, R. Sgammato, A. Lamberti, R. Arcone, R. Salerno, M. Nardi, M. Masullo and M. Oliverio, *ACS Med. Chem. Lett.*, 2016, **7**, 470–475.

45 B. Kuzu, M. Tan, P. Taslimi, İ. Gülçin, M. Taşpınar and N. Menges, *Bioorg. Chem.*, 2019, **86**, 187–196.

46 A. Daina, O. Michielin and V. Zoete, *Sci. Rep.*, 2017, **7**, 42717.

47 B. N. Sağlık, S. Levent, D. Osmaniye, A. E. Evren, A. B. Karaduman, Y. Özkay and Z. A. Kaplancıklı, *ACS Omega*, 2022, **7**, 47378–47404.

48 D. Osmaniye, A. E. Evren, B. N. Sağlık, S. Levent, Y. Özkay and Z. A. Kaplancıklı, *Arch. Pharm.*, 2022, **355**, 2100450.

49 D. Osmaniye, B. Korkut Çelikateş, B. N. Sağlık, S. Levent, U. Acar Çevik, B. Kaya Çavuşoğlu, S. Ilgın, Y. Özkay and Z. A. Kaplancıklı, *Eur. J. Med. Chem.*, 2021, **210**, 112979.

50 L. Schrödinger, *LigPrep. Version, 3*, 2016, New York, NY, USA, 2012.

51 *Release, S. 2: LigPrep, version 3.8*, Schrödinger, 2016.

52 L. Schrödinger, *Glide, Version 7.1*, Schrödinger, LLC, New York, NY, USA, 2016.

53 X. Liu, D. Shi, S. Zhou, H. Liu, H. Liu and X. Yao, *Expet Opin. Drug Discov.*, 2018, **13**, 23–37.

54 *M.-D. I. Tools*, Schrödinger, LLC, New York, NY, 2020, Schrödinger Release 2018-3: Prime, 2018.

55 S. Release, *1: Desmond Molecular Dynamics System*.

56 D. D. Humphreys, R. A. Friesner and B. J. Berne, *J. Phys. Chem.*, 1994, **98**, 6885–6892.

57 G. J. Martyna, D. J. Tobias and M. L. Klein, *J. Chem. Phys.*, 1994, **101**, 4177–4189.

58 W. G. Hoover, *Phys. Rev. A*, 1985, **31**, 1695–1697.

59 U. Essmann, L. Perera, M. L. Berkowitz, T. Darden, H. Lee and L. G. Pedersen, *J. Chem. Phys.*, 1995, **103**, 8577–8593.